

## XRD study on the structural evolution of Zn-exchanged titanosilicate ETS-4 during thermal treatment

V. Kostov-Kytin<sup>1\*</sup>, R. Nikolova<sup>1</sup>, G. Avdeev<sup>2</sup>

<sup>1</sup> Bulgarian Academy of Sciences, Institute of Mineralogy and Crystallography “Acad. Ivan Kostov”, 1113 Sofia, Akad. G. Bonchev Str., bl. 107, Bulgaria

<sup>2</sup> Bulgarian Academy of Sciences, Institute of Physical Chemistry “Rostislav Kaischew”, 1113 Sofia, Akad. G. Bonchev Str., bl. 11, Bulgaria

Received October 07, 2018; Accepted November 30, 2018

*In situ* time-resolved powder X-ray diffraction technique has been applied to investigate the structural evolution of Zn-exchanged polycrystalline titanosilicate ETS-4 upon heating within the temperature interval from 25 to 375 °C. The facilities of the Rietveld method as implemented in the software package GSAS have been used to control the plausibility of the obtained crystal-chemical characteristics at each stage. Previous single crystal structure determination of the title compound has served as initial model for the refinement procedure held on a sample at room temperature. Subsequently, the structure model of each increasing temperature step has been taken from the previous refinement. The structural evolution has been evaluated in terms of the unit cell parameters changes, water molecules site occupancies (during the dehydration period), the titano-silicate framework flexibility (pore sizes), and possible atomic motion during the thermal treatment. The obtained results and previously accumulated knowledge on the crystal-chemical peculiarities of ion-exchanged ETS-4 and its behavior upon heating have been interpreted in terms of the elastic properties of this titanosilicate structure and its thermal stability.

**Keywords:** Zn-ETS-4, Rietveld refinement, structural evolution.

### INTRODUCTION

The synthetic zeolite-like titanosilicate ETS-4 (Engelhard Titanium Silicate-4), was patented by Kuzniki et al. in 1989 and 1990 [1, 2]. Since then the interest of the scientific community towards preparation of microporous and layered titanosilicates with potential application in various areas of technology such as catalysis, gas separation, energy storage, optoelectronics, radioactive waste management, etc has steadily increased. ETS-4 has as a natural analogue the mineral zorite with ideal chemical formula  $\text{Na}_6\text{Ti}_5\text{Si}_{12}\text{O}_{34}(\text{O},\text{OH})_5 \cdot 11\text{H}_2\text{O}$  [3, 4]. Sandomirskii and Belov recognized the order-disorder (OD) character of zorite structure and solved its superposition (family) structure in the space group Cmmm [4]. The averaged structure model of these authors is also applicable to ETS-4 materials (as-synthesized and ion-exchanged forms). It can be described as consisting of chains of TiO<sub>6</sub> octahedra (Ti1) parallel to the [010] direction laterally linked

by a chain of four SiO<sub>4</sub> tetrahedra along [100] direction. These SiO<sub>4</sub> groups are linked in [010] direction by a chain-bridging unit including the Ti(2) site with statistically reverted polarity of its polyhedron (Fig. 1). An interesting peculiarity is the coordination of Ti(2) atom. Some authors have found evidences for the hemi-octahedral coordination of Ti in the chain-bridging site and other support its six-coordination. Detailed discussion on this is presented by M. Sacerdoti and G. Cruciani in 2011 [5]. Both ETS-4 and zorite are disordered crystalline materials, being faulted in the [100] and [001] directions. Crystallographically, their structure is described as an intergrowth of four polytypes which differ in the stacking of the titanosilicate bridging units in the [100] and [001] directions [6, 7]. Such disorder blocks the 12-membered rings along the c direction (Fig. 1a), and as a result, the transport is controlled by limiting 8-membered ring openings running along [010] (Fig. 1b).

The ion-exchange forms of zorite and ETS-4 have been studied by several authors [6–14]. Summarizing some of the results in these works in 2011 Spiridonova et al. [11, 15] classified the extra-framework cation sites into three groups denoted as

\* To whom all correspondence should be sent:  
E-mail: vkytin@abv.bg

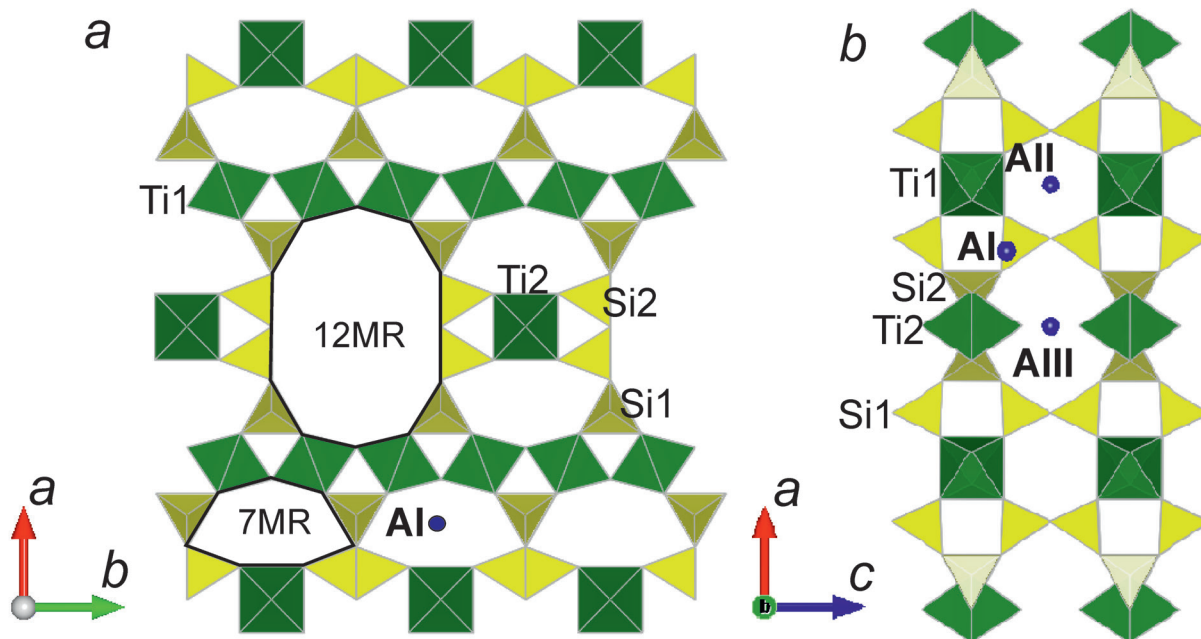


**Fig. 1.** A view of the ETS-4 structure projected along [001] (a) and along [010] (b). Extra-framework species have been omitted for clarity.

Al, AlI, AlII, AlIII (Fig. 1b). The same authors demonstrated how the degree of cation exchange depends upon the experimental conditions. Subsequent structural investigations of ion-exchange forms of the synthetic material supported this classification scheme including new species in it (e.g.  $\text{Zn}^{2+}$  and  $\text{Mg}^{2+}$ ) [12–14].

Over the years, the thermal stability of these materials has also been intensively studied. Naderi and Anderson (1996) described for ETS-4 a series of transformations upon heating including a partial structure rearrangement at ca. 200 °C, followed by complete amorphization at 500 °C, formation of a new layered material at 600 °C, and then of highly crystalline narsarsukite at 700 °C [16]. According to Rocha and Anderson (2000) the collapse of Na-ETS-4 to an amorphous near 200 °C was due to the loss of structural water chains present along the channel systems [17]. Although Na-form of ETS-4 is thermally unstable, it has been suggested that the ion exchange with divalent cations such as  $\text{Sr}^{2+}$ ,  $\text{Ba}^{2+}$ ,  $\text{Ca}^{2+}$ ,  $\text{Mg}^{2+}$ , etc., would enhance the thermal stability [6, 20]. A detailed neutron powder diffraction and spectroscopic study was carried out by Kuznicki et al. (2001) and Nair et al. (2001b) on samples of Sr-exchanged ETS-4 heated *ex situ* at selected temperatures between 150 °C and 300 °C and showed that Sr-ETS-4 withstands thermal dehydration up to 350 °C [18,19]. In [18] S.M. Kuznicki et al. (2001) suggested a plausible mechanism for

the loss of order in Sr-exchanged ETS-4 treated at temperatures higher than 250 °C as registered in the powder X-ray and neutron diffraction patterns. The authors have noticed that reflections with a  $k$  component broaden and disappear first upon heating and interpreted that as an indication for deformations and eventual breaking of the titania chains that run along the  $b$  axis. Our unpublished investigations give ground to consider that the crystal structures of  $\text{Ba}^{2+}$ - and  $\text{Cs}^{+}$ -exchanged forms remain intact at temperatures above 400 and 450 °C, respectively.

The framework flexibility of the investigated materials upon contraction or expansion have also attracted the specialists attention as it provides opportunity to adjust the effective size of the pores and increase its size-selectivity in the gas adsorption applications and purification of water containing organic and inorganic pollutant. This has been duly demonstrated on the example of thermally treated Sr-exchanged ETS-4 by Nair et al. (2001) [19] who applied for this Rietveld analysis as implemented in the GSAS Rietveld refinement package [21, 22]. The so-obtained material (called CTS-1, Contracted TitanoSilicate-1) has been patented by Kuznicki [20, 23–24]. In 2011 M. Sacerdoti and G. Cruciani reported results from comparing the structural modifications, including the transient states, underwent by zorite and Na-ETS-4 when dynamically (continuously) heated up to 400 °C. They were achieved by means of temperature-resolved *in situ*

powder diffraction using synchrotron radiation and Rietveld refinement [5]. S. Ferdov (2010) has used similar approach to evaluate the dimensions and the reversibility of the temperature- and vacuum-induced framework contractions of polycrystalline Na-ETS-4 [25].

The present study provides new knowledge on the ion-exchange properties of ETS-4 material and its structural evolution upon thermal treatment on the example of its Zn-exchanged form heated up to 450 °C. The obtained results and previously accumulated knowledge on the crystal-chemical peculiarities of ion-exchanged ETS-4 and its behavior upon heating have been interpreted in terms of the elastic properties of this titanosilicate structure and its thermal stability.

## EXPERIMENTAL

### *Synthesis and ion exchange*

ETS-4 polycrystalline samples were synthesized according to a previously reported procedure [26]. For structural determination and elucidation of the positions of the Zn<sup>2+</sup> ions, single crystals of ETS-4 have been prepared [27]. The ion exchange was performed by immersing the as-synthesized ETS-4 samples, in 1 M solutions of ZnCl<sub>2</sub> (Aldrich) for 3 days at 90 °C. Finally, the samples were washed several times (5–7) by distilled water (around 300 ml H<sub>2</sub>O per 0.5 g of solid product) and dried at room temperature.

### *Analytical procedure*

The initial powder X-ray diffraction (PXRD) patterns of the as-synthesized polycrystalline sample – (Na,K)-ETS-4 and of the same material exchanged on Zn were collected on Bruker D2Phaser diffractometer with Ni-filtered CuK $\alpha$  radiation in the 2 $\theta$  range from 5 to 70° and in a step-scan regime (step 0.015° and time 10 s per step). The single crystal data were collected on an Agilent Diffraction SuperNovaDual four-circle diffractometer equipped with an Atlas CCD detector using mirror-monochromatized Mo-K $\alpha$  radiation from a micro-focus source. The time resolved PXRD measurements were collected at PANalytical Empyrean equipped with a multichannel detector (Pixel 3D) using (Cu K $\alpha$  45 kV–40 mA) radiation in the 10–100° 2 $\theta$  range, with a scan step of 0.01° for 24 s. The *in situ* HT-XRD measurements were carried out by means of an Anton Paar HT-16 camera with a sample directly heated with a heating filament from room temperature to 500 °C. All experiments were conducted on air with heating rate of about 5 °C per minute.

### *Structure refinements: methods, approach and visualization*

The Rietveld analyses were performed using the GSAS-EXPGUI suite of programs (Larson and Von Dreele 1994; Toby 2001) [21, 22]. The WinPLOTR utilities as a Windows tool for powder diffraction patterns analysis have been used for certain graphic presentations [28]. Visualizations of crystal structures and structural motifs have been performed with VESTA 3 software [29].

The crystal structure of Zn-exchanged ETS-4 single crystals (depository number ICSD: 425400, [13, 30]) was used to prepare the starting model for the refinement procedure held on samples of preliminary exchanged on the same metal polycrystalline material at room temperature. It is worth noting that in this model the titanium (Ti2) from the chain-bridging unit is six-coordinated. Already at this stage it became clear that the imposed model of completely substituted on Zn ETS-4 should meet the complexity of the refined profile curve caused by the presence of phase impurities and possibly non-exchanged portions of the studied titanosilicate phase. A possible indication for the latter is a reflection registered at 26.05 2 $\theta$ , (°) coinciding with the (601) peak of the unreacted material unless not recognized as an unidentified impurity. The strongest reflection of another concomitantly synthesized with ETS-4 titanosilicate phase – GTS-1 with ideal formula M<sub>3</sub>H(TiO)<sub>4</sub>(SiO<sub>4</sub>)<sub>3</sub>·4H<sub>2</sub>O (M=K, Na) has also been registered at 11.42 (100) 2 $\theta$ , (°) [26]. The picture gets even more complicated during the *in situ* time resolved high temperature investigations due to the impact of the platinum substrate used in the experiments and manifested by the presence of Pt strongest reflections at 39.75 (111), 46.23 (200), 67.45 81.24 (220), (311), 85.68 (222) 2 $\theta$ , (°). To partially solve the problem the listed reflections and phases have been excluded from the refinement procedure at all temperature steps the more so because the thermal expansion affects them differently. During the subsequent Rietveld procedures, the structure model of each increasing temperature step has been taken from the previous temperature step refinements. This study presents the results obtained for samples heated at 25, 125, 225, 325, and 375 °C. Although Zn-ETS-4 showed some residual crystallinity at temperatures above 400 °C, the low number of reflections did not allow any Rietveld refinement for the samples in these conditions. For all temperature steps: the Bragg peak profile was modelled using a pseudo-Voigt function with a 0.01% cut-off of the peak intensity; the background curve was fitted using a Chebyshev polynomial with 24 variable coefficients; scattering curves of neutral atoms were used; soft constraints were imposed on

Ti-O and Si-O distances, and the same weight was used throughout the refinement procedure.

In GSAS the so called “soft constraints” or “restraints” are used. This provides opportunity for the scientists who wish to “push” the model towards certain expectations (for example, bond lengths). Their application requires specification of tolerance range for the values of each expectation. Each expectation is weighted by the uncertainty (sometimes s.u. or E.S.D.) for the expectation as well as the overall Restraint Weighting factor (RWf). The smaller the uncertainty and the larger Restraint Weighting factor, the stronger the model is “pushed” towards following the expectation. Soft constraints affect the refinement and their relative contribution to the total  $\chi^2$  in the final stages of refinement procedure should be reported.

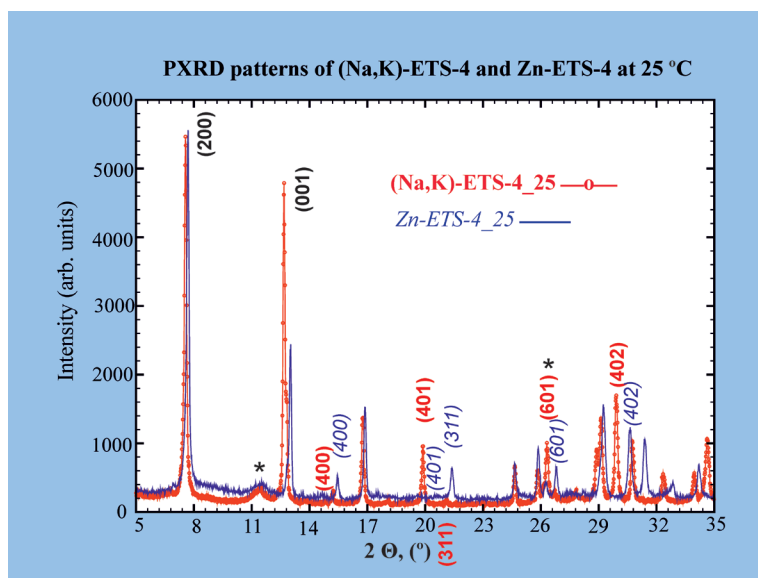
Thus, taking into account the complexity of the refined profile curve the appropriate choice of soft constraints parameters (type, individual expectations tolerance, and overall weight) is a compromise between the opportunities to inspect certain crystal structure deviations e.g. elasticity in terms of bond lengths and angles and the plausibility of the finally received crystal-chemical parameters. After preliminary trials in this study the overall RWf has been fixed to 1000 for all stages of the refinement. All data in the following sections are obtain for this value unless otherwise stated (see Table 4.).

Each cycle of refinements concerning a certain temperature step has been followed by a peak search procedure applying difference Fourier “DELF” calculations with program FORSCH as implemented

in the GSAS program software. Special attention has been paid to the behavior of the extra-framework species.

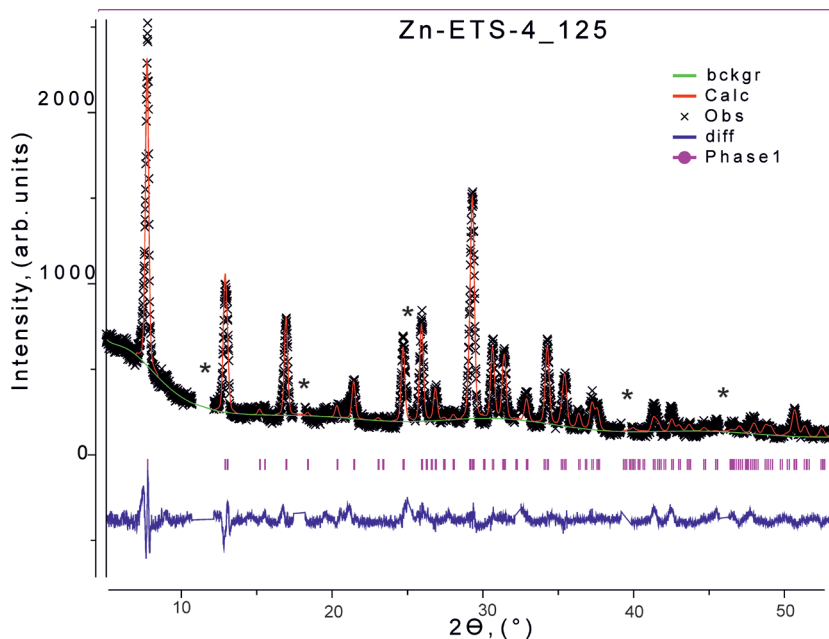
## RESULTS

Figure 1 presents the crystal structure of the ETS-4 synthetic titanosilicate derived from that one of the mineral zorite according to the average structure model of Sandomirskii and Belov. It illustrates the blocked 12-membered rings (12MR) channels in the [001] direction (Fig 1a) and the 8- and 6-membered rings (8MR, 6MR) running along the [010] direction (Fig. 1b). Figure 1b also depicts the positions of the classified into three groups by Spiridonova et al. [11, 15] extra-framework cation sites denoted as AI, AII, AIII. Figure 2 gives comparison between the PXRD patterns of the initial polycrystalline (Na,K)-ETS-4 sample and that one of the exchanged on Zn material at 25 °C. Some of the most noticeable differences in terms of reflections position shifts and intensity changes are designated correspondingly for the two forms. Figure 3 presents Rietveld refinement for Zn-exchanged polycrystalline ETS-4 material heated at 125 °C. Figures 4 and 5 give notion for the 8MR and 6MR channels running along the [010] and their apertures with respect to the *a*-axis. Table 1 presents positional and thermal parameters of the atoms in the structure of Zn-ETS-4 at 25 °C as obtained from the *in situ* time resolved powder X-ray diffraction experiment. Table 2 provides data on the lattice parameters and refinement



**Fig. 2.** PXRD patterns of the as-synthesized polycrystalline (Na,K)-ETS-4 sample and that one of the exchanged on Zn material at 25 °C. The asterisks denote impurity phases or unreacted initial phase (see the Structure refinements section).





**Fig. 3.** Rietveld refinement for the Zn-ETS-4 sample heated at 125 °C. The experimental XRD data are denoted with x-symbols; the line through the markers is the result from the refinement; the Bragg positions are shown as short vertical lines; at the bottom is the difference plot between the data and the calculated profile; the asterisks mark the excluded from the refinement regions (see the Structure refinements section).

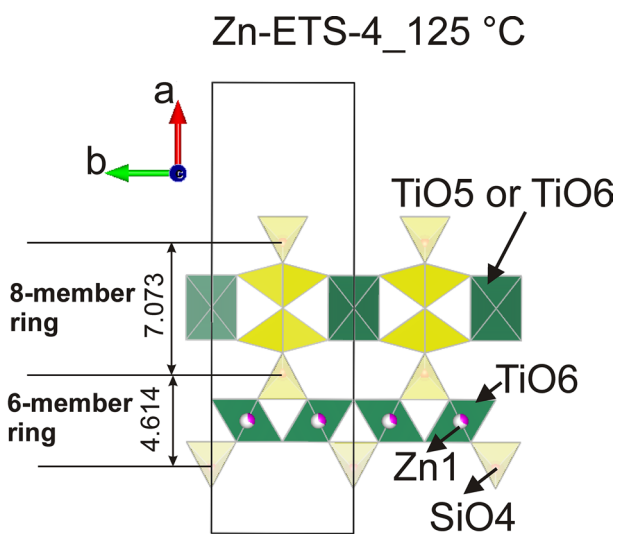


**Fig. 4.** View of the 8MR and 6MR channels running along the [010] and their apertures with respect to the a-axis for the Zn-ETS-4 sample heated at 125 °C.

details for selected Zn-exchanged ETS-4 samples within the temperature range 25–375 °C. Table 3 presents selected bond distances (Å) for the studied Zn-exchanged ETS-4 at RWf = 1000. Figure 6 illustrates the 8MR and 6MR contractions and expansions during the thermal treatment (RWf = 1000). Table 4 presents data demonstrating the impact of

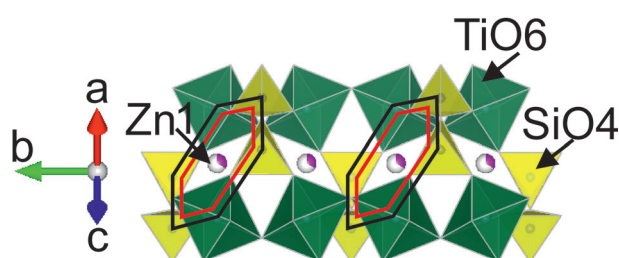


**Fig. 5.** Topology of the 6MR channels running along the [010] with positions of the residing there Zn1.

the overall Restraint Weight factor choice on the measured dimensions on the example of the 8MR and 6MR for Zn-ETS-4 heated at 375 °C. Figure 7 compares the PXRD patterns of Zn-ETS-4 heated at 25 and 325 °C. Figure 8 presents the 6MR channels topology of Zn-ETS-4 at 25 and 375 °C along [010]. The position of the “DELFI” map strongest peak ( $\rho = 4.225$ ,  $x = 0.2432$ ,  $y = 0.3816$ ,  $z = 0.5000$ ) obtained after refinement procedures and application of the program FORSCH for the sample heated at 375 °C is designated there as Ti1-1.

## DISCUSSION

Figure 2 illustrates the extent of the ion-exchange process for the studied compound in terms

**Table 1.** Positional and thermal parameters of the atoms in the structure of Zn-ETS-4 at 25 °C as obtained from the *in situ* time resolved powder X-ray diffraction studies

Atom	x	y	z	Sof	U <sub>equiv</sub> , Å <sup>2</sup> ***
Zn1	1/4	1/4	0	0.313(7)	0.057(5)
Zn2	0.3767(5)	0	0.382(3)	0.434(4)	0.059(9)
Si1	0.1622(4)	0	0.232(2)	1	0.039(2)
Si2	0.0668(8)	0.070(2)	1/2	0.5**	0.055(5)
Ti1	1/4	1/4	1/2	1	0.052(3)
Ti2	0	1/2	1/2	0.5**	0.060(8)
O1	0.129(2)	0	0	1	0.025(4)
O2	0.1920(7)	0.195(1)	0.318(3)	1	0.060(3)
O3	0.0946(8)	0	0.286(4)	1	0.075(7)
O4	0	0	0.447(3)	1	0.08(2)
O5	0.067(1)	0.3210 f*	1/2	0.5**	0.09(2)
O6	0.285(1)	0	1/2	1	0.060(8)
O7	0	1/2	0.184(6)	0.5**	0.09(6)
O21	0.310(2)	0	0	0.87(2)	0.07(2)
O22	0	0.385(7)	0	0.73(2)	0.21(6)
O23	0	0	0.16(1)	0.50(2)	0.09(4)

O21, O22, O23 – water molecules;

f\* position is fixed during the refinement procedure;

\*\* fixed occupancies as taken from the model obtained from the single crystal investigations (not included in the refinement);

\*\*\* values taken from the single crystal investigations (not included in the refinement).

**Table 2.** Lattice parameters and refinement details for Zn-exchanged ETS-4 samples within the temperature range 25–375 °C.

	In situ time resolved powder X-ray diffraction studies (selected samples)				
	Zn-ETS-4 at 25 °C	Zn-ETS-4 at 125 °C	Zn-ETS-4 at 225 °C	Zn-ETS-4 at 325 °C	Zn-ETS-4 at 375 °C
<i>Space Group</i>	<i>C mmm</i>	<i>C mmm</i>	<i>C mmm</i>	<i>C mmm</i>	
<i>a</i> (Å)	22.943(3)	22.841(3)	22.689(3)	22.419(7)	22.12(2)
<i>b</i> (Å)	7.2241(7)	7.2067(5)	7.2401(6)	7.238(1)	7.236(4)
<i>c</i> (Å)	6.8081(8)	6.7899(6)	6.7556(6)	6.701(1)	6.644(4)
V (Å) <sup>3</sup>	1128.4(3)	1117.7(2)	1109.7(2)	1087.4(6)	1063(2)
Rwp (%)	15.03	9.88	8.99	11.51	12.88
Rp (%)	11.11	8.41	7.72	9.46	10.84
Red- $\chi^2$	3.511	2.400	2.024	2.256	2.560
N <sub>obs</sub>	5830	6034	6044	5966	6043
RF <sup>2</sup> (%)	24.35	21.89	16.24	16.61	42.13
N <sub>var</sub>	60	60	60	58	41
No restraints	20	20	20	20	20
Total restraint $\chi^2$ contribution	6.68 each	5.89 each	7.07 each	10.15 each	23.45 each

$$Rp = \sum [Y_{io} - Y_{ic}] / \sum Y_{io}; Rwp = [\sum wi(Y_{io} - Y_{ic})^2 / \sum wiY_{io}^2]^{0.5}; RF^2 = \sum |Fo^2 - Fc^2| / \sum |Fo^2|;$$

$$Red-\chi^2 = \sum wi(Y_{io} - Y_{ic})^2 / (N_{obs} - N_{var})$$

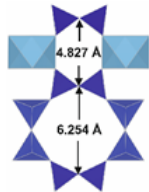
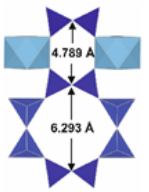
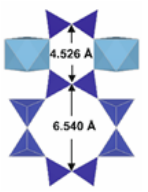
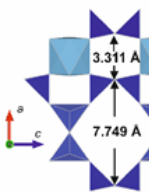
Estimated standard deviations in parentheses refer to the last digit.

**Table 3.** Selected bond distances (Å) for Zn-exchanged ETS-4 samples obtained within the temperature range 25–375 °C

	In situ time resolved powder X-ray diffraction studies (selected samples, Rwf = 1000)				
	Zn-ETS-4 at 25 °C	Zn-ETS-4 at 125 °C	Zn-ETS-4 at 225 °C	Zn-ETS-4 at 325 °C	Zn-ETS-4 at 375 °C
Si1-O1	1.75(2)	1.58(1)	1.56(1)	1.54(2)	1.62(3)
Si1-O2[x2]	1.68(1)	1.63(1)	1.61(1)	1.63(2)	1.94(2)
Si1-O3	1.59(2)	1.52(2)	1.47(2)	1.52(3)	1.71(4)
Si2-O3[x2]	1.67(2)	1.68(2)	1.72(2)	1.59(3)	1.66(3)
Si2-O4	1.61(2)	1.47(2)	1.38(1)	1.50(3)	1.59(3)
Si2-O5	1.82(2)	1.73(1)	1.76(2)	1.82(3)	1.85(5)
Ti1-O2[x4]	1.86(1)	1.88(1)	1.89(1)	1.91(2)	1.96(3)
Ti1-O6[x2]	1.98(1)	2.04(1)	2.08(1)	2.23(2)	2.29(3)
Ti2-O5[x4]	2.00(2)	2.11(2)	2.09(2)	2.09(2)	2.01(2)
Ti2-O7[x2]	2.14(4)	2.11(4)	2.09(3)	2.04(3)	2.05(4)
					2.45(5)
Zn1-O2[x4]	2.57(2)	2.30(2)	2.25(1)	2.11(2)	2.24(4)
Zn1-O21[x2]	2.224(2)	2.360(2)	2.45(2)	–	–
Zn2-O2[x2]					2.45(4)
Zn2-O5[x2]	2.07(2)	1.95(2)	1.96(2)	2.16(1)	2.18(1)
Zn2-O6	2.22(3)	2.03(2)	1.91(2)	2.09(3)	2.14(4)
Zn2-O7					2.612(9)

Note: Estimated standard deviations in parentheses refer to the last digit. For E.S.D. meaning obtained for the restrained bond distances (Ti-O and Si-O) see the *Structure refinements* section.

**Table 4.** Impact of the overall Restraint Weighting factor (Rwf) value on measured dimensions for Zn-ETS-4 at 375 °C

	Rwf = 10 000	Rwf = 5 000	Rwf = 2 000	Rwf = 1 000
Apertures of the 8MR and 6MR channels with respect to the <i>a</i> -axis (Å)				
Rwp (%)	13.56	13.41	13.22	12.88
Rp (%)	11.42	11.26	11.11	10.84
Red- $\chi^2$	2.68	2.65	2.605	2.56
No <sub>var</sub>	41	41	41	41
No restraints	20	20	20	20
Total restraint $\chi^2$ contribution	10.98	14.45	15.53	23.45
	Lattice parameters			
<i>a</i> (Å)	22.16(2)	22.15(2)	22.13(2)	22.12 (2)
<i>b</i> (Å)	7.211(4)	7.215(4)	7.220(4)	7.236(4)
<i>c</i> (Å)	6.651(4)	6.649(4)	6.646(4)	6.644(4)
	Selected bond distances (Å)			
Si1-O1	1.57(2)	1.61(2)	1.65(3)	1.62(3)
Si1-O2[x2]	1.60(1)	1.66(2)	1.75(2)	1.94(2)
Si1-O3	1.51(2)	1.51(3)	1.49(4)	1.71(4)
Si2-O3[x2]	1.67(1)	1.69(3)	1.72(2)	1.66(3)
Si2-O4	1.61(2)	1.58(2)	1.55(3)	1.59(3)
Si2-O5	1.65(2)	1.65(2)	1.70(4)	1.85(5)
Ti1-O2[x4]	2.082(9)	2.07(1)	2.04(2)	1.96(3)
Ti1-O6[x2]	2.14(1)	2.17(2)	2.24(2)	2.29(3)
Ti2-O5[x4]	2.064(8)	2.06(1)	2.05(2)	2.01(2)
Ti2-O7[x2]	2.07(1)	2.07(2)	2.07(3)	2.05(4)

Note: Estimated standard deviations in parentheses refer to the last digit. For E.S.D. meaning obtained for the restrained bond distances (Ti-O and Si-O) see the *Structure refinements* section.

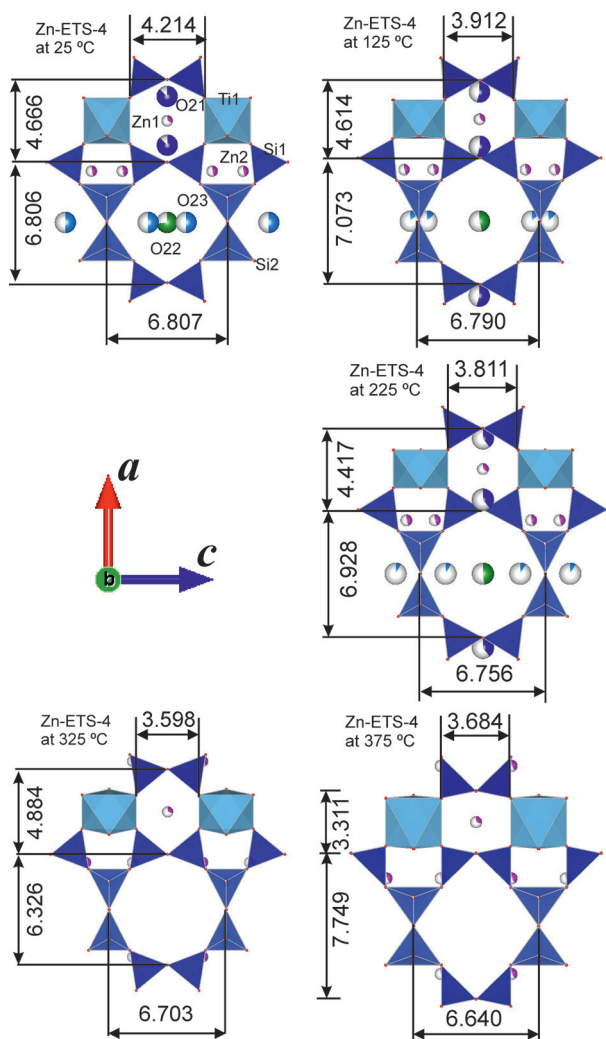


**Fig. 6.** Aperture dimensions, (Å) of the 8MR and 6MR of Zn-ETS-4 heated at different temperatures and measured (RWF = 1000) along the a- and c-axes. The pie chart type of circles filling applied for the extra-framework species corresponds to the refined occupancy of these sites.

of certain reflections position shifts and intensity changes. The PXRD profile of Zn-ETS-4 has well been fitted with the calculated one from the starting structural model with the exception of the reflection registered at  $26.05\ 2\theta$ , ( $^\circ$ ) coinciding with the (601) peak of the unreacted material. It may as well belong to an impurity phase. As it has been explained in the Experimental sections certain  $2\theta$  regions of the PXRD patterns have been excluded from the fitting procedures (Fig. 3).

According to the initial structural model and the subsequent Rietveld refinements  $Zn^{2+}$  occupies positions AI and AII. Zn1 resides in the 6MR channels (Fig. 4 and Fig. 5) whereas Zn2 can be detected in the 7MR channels running along [001] (see Fig. 1a). Part of the water molecules occupy the 8MR chan-

nels, the rest is in the 6MR channels. Data in Table 2 support the correctness of the initially chosen structural model for the refinements of all studied samples with the exception of that one heated at  $375\ ^\circ C$ . The observed by previous investigators structure shrinkage upon heating has also been registered, here in terms of lattice parameters values.

Upon heating the water molecules exhibit positional shifts and logical decrease of site occupancy (Fig. 6). No water is present in Zn-ETS-4 after  $300\ ^\circ C$ . On their side both Zn1 and Zn2 are more stationary. Attempts have been made to increase the multiplicities of their sites thus providing opportunity for motion. In general, under the chosen refinement conditions any attempts to register substantial  $Zn^{2+}$  motions within the temperature range  $25\text{--}325\ ^\circ C$  by applying program FORSCH failed. Table 3 data indicate that the Zn-O distances decrease when temperature rises reaching boundary levels. This leads to the suggestion that in these circumstances they act more as framework cations hindering and slowing up the structural collapse. The experimental data revealed that the most elastic part of the ETS-4 structure appeared to be the 8MR built of  $SiO_4$  tetrahedra. Figure 6 illustrates their expansion and shrinkage during the dehydration process and subsequent thermal expansion in the [100] direction. Similar behavior has already been observed for Sr-ETS-4 [19], Na-ETS-4 and zorite [5]. Nair et al. (2001b) noted that beyond  $200\ ^\circ C$ , the dimension D2 (along the a-axis diameter of the 8MR in the Sr-exchanged form) expands relatively, so that the 8MR distorts from an “octagonal” toward a “quadrilateral” cross section just the same as for Zn-ETS-4 at  $375\ ^\circ C$  in this study (Fig. 6). Probably, this should have happened at the earlier stages of thermal treatment provided that more precise and accurate experimental data have been processed. The role of the overall Restraint Weight should also be taken into account. Its impact over the final results is demonstrated in Table 4 on the example of Zn-ETS-4 at  $375\ ^\circ C$ . Anyway the obtained in this study results support the tendencies observed from previous investigations in terms of the unit cell parameters changes, water molecules site occupancies (during the dehydration period), and the titano-silicate framework flexibility (pore sizes) of ETS-4 materials upon heating.

At  $375\ ^\circ C$  the refinement results are already indicative for onset of structural breakdown. The “DELFI” map strongest peak ( $\rho=4.225$ ) positioned at  $x = 0.2432$ ,  $y = 0.3816$ ,  $z = 0.5000$  has been recognized as shifted Ti1 (see Table 1) and the fact has been interpreted as breaking of the Ti-O-Ti chains running along [010] thus initiating the subsequent structural collapse. Kuznicki et al. (2001) foresaw such scenario when discussing the observed by them broadening and disappearing of the reflections with



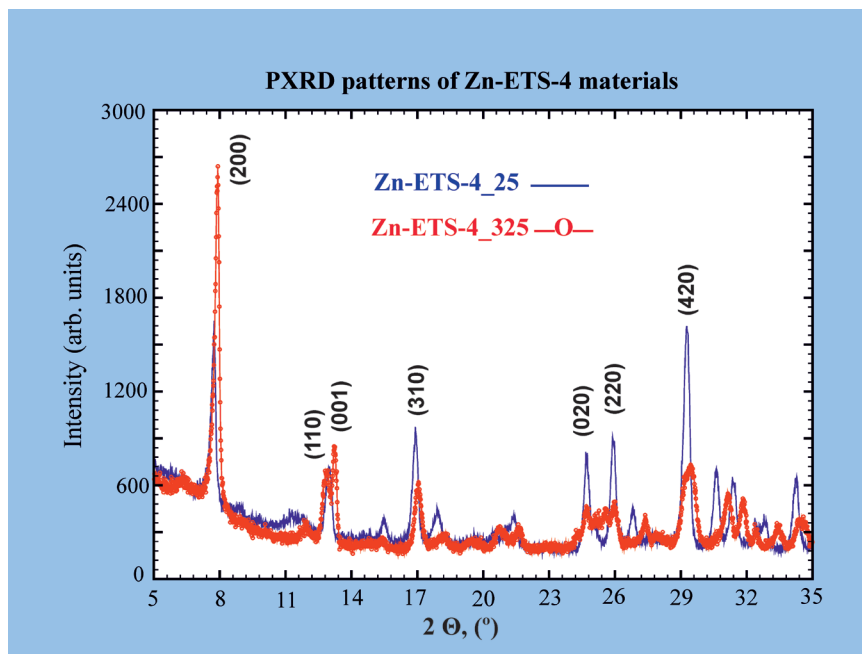


Fig. 7. PXRD patterns of Zn-ETS-4 samples at 25 and 325 °C.

a  $k$  component  $\neq 0$  [18]. In this study this is demonstrated in Fig. 7. It is seen there that reflections (200) and (001) have increased their intensities as a result of the dehydration process. This comes as a direct effect of the loss of water molecules over the absolute value of the structure factor for these directions. Substantial broadening is registered for the rest of the reflections at 325 °C as compared with the room temperature experiment. Figure 8 gives notion for the occurring upon heating structural deformations related with the expansion of the 8-membered  $\text{SiO}_4$  rings. The latter mostly affect dimensions of the  $\text{TiO}_6$  octahedra forming chains along [010]. That is why it is supposed here that the subsequent structural collapse starts by positional shift of Ti1 (as illustrated in Fig. 8 by the position of the strongest peak obtained from the program FORSCH and designated there as Ti1-1) followed by breaking of certain Ti-O linkages.

#### *Considerations for the thermal stability of ion-exchanged-ETS-4 materials*

The 12MR channels in ETS-4 are precluded by randomly positioned titanosilicate bridging units and this makes the 8MR channels the main pathway for ion-exchange and water sorption/release in the structure of the studied materials. Like other microporous compounds the cation uptake of ETS-4 depends on its theoretical capacity, experimental

conditions of exchange, and the cation characteristics (ionic size, charge). The latter is a crucial factor controlling the penetration of the species either directly in the 6MR channels taking into consideration their effective diameter or passing there from the 8MR channels through openings in the  $b$ - $c$  plane.

In most of the up to now studied ion-exchanged forms of the synthetic titanosilicate ETS-4 the cation species occupy the 6MR and 7MR channels i.e. positions AI and AII [11, 15] (Fig. 1). Exception is  $\text{Cs}^+$  which occupies the AIII position [27]. For the natural counterpart of ETS-4 – the mineral zorite, Spiridonova et al. (2011) reported for the AIII site also  $\text{Rb}^+$ ,  $\text{Tl}^+$ , and  $\text{Ag}^+$ . In general for ETS-4, cations with ionic radii of up to 1.3 Å or less occupy the 6MR channels (Na, Mg, Ag, Zn (this study), Ni, Cu, Mn (unpublished data)). The bigger ones reside in positions AII (e.g. Ag, Sr, and Ba) and AIII (Cs). This fact offers interesting aspects concerning the thermal stability of the studied material. Provided that the 8MRs built of  $\text{SiO}_4$  tetrahedra are the most elastic unit in the structure, then the type (in terms of ionic size and charge) and position of the extra-framework cations can be used to control their effective diameter during heat treatment. Thus, the bigger cations residing within the 8MR channels can restrict from inside their thermal expansion by reaching boundary values of their bonds with the framework oxygen. Our preliminary unpublished data give evidence for the stability of the Cs-form

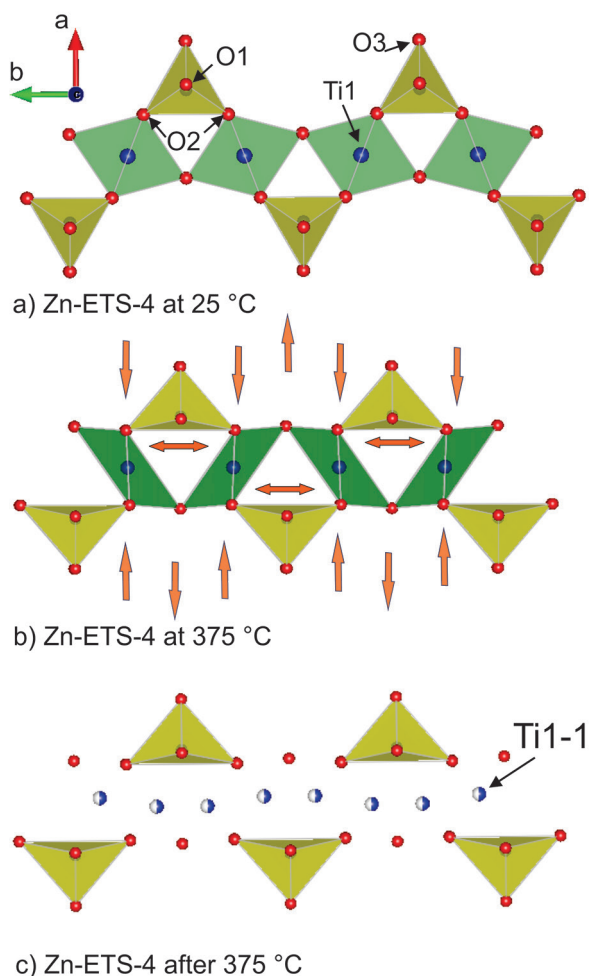


**Fig. 8.** 6MR channel topologies of Zn-ETS-4 at 25 and 375 °C. The arrows denote direction of forces causing structural deformations. Position of the strongest peak obtained from the program FORSCH is designated as Ti1-1.

up to 450 °C. On the other hand, the cation species from the 6MR channels withstand such expansion from outside the 8MR. The bigger their sizes and the stronger their bonds with the framework oxygens the slower the enlargement of 8MRs and the contraction of 6MRs and the subsequent structural collapse. The same is the action of the cations positioned in AII.

Such data can be used for tailoring of new materials for selective adsorption based on appropriately ion-exchanged forms of ETS-4 and heated within a definite temperature range.

## CONCLUSIONS

The present study provides new knowledge on the ion-exchange properties and characteristics of

the synthetic titanosilicate ETS-4 on the example of its Zn-exchanged form.

The facilities of the Rietveld analysis as implemented in program GSAS have been demonstrated as a powerful means for investigation of the structural evolution of the studied and similar materials upon thermal treatment. In this work it has been evaluated in terms of the unit cell parameters changes, water molecules site occupancies (during the dehydration period), the titano-silicate framework flexibility (pore sizes), and possible atomic motion.

The obtained results and previously accumulated knowledge on the crystal-chemical peculiarities of ion-exchanged ETS-4 and its behavior upon heating have been interpreted in terms of the elastic properties of this titanosilicate structure and its thermal stability.

The obtained data can be used for design of new materials based on their appropriately chosen ion-exchanged forms and systematically contracted microporous framework upon heat treatment in order to adjust their effective pores sizes and to increase their size-selectivity in e.g. gas adsorption applications.

**Acknowledgements:** This work was financially supported by the National Science Fund of Bulgaria under contract No. DNTS/Russia 02/8 from 15.06.2018.

## REFERENCES

1. S. M. Kuzniki, *US Patent* 4:853–202, (1989).
2. S. M. Kuzniki, *US Patent* 4:938–989, (1990).
3. A. N. Mer'kov, I. V. Bussen, E. A. Goiko, E. A. Kul'chitskaya, Yu. P. Men'shikov, A. P. Nedorezova, *Zap VMO*, **102** (1), 54 (1973) (in Russian).
4. P. A. Sandomirskii, N. V. Belov, *Sov. Phys. Crystallogr*, **24**, 686, *Kristallografiya*, **24**, 1198 (1979).
5. M. Sacerdoti, G. Cruciani, in: *Minerals as Advanced Materials II.*, Springer, S. V. Krivovichev (ed), Springer Heidelberg New York Dordrecht London, 2011, p. 187.
6. C. Braunbarth, H. W. Hillhouse, S. Nair, M. Tsapatis, A. Burton, R. F. Lobo, R. M. Jacubinas, S. M. Kuznicki, *Chem. Mater.*, **12**, 1857 (2000).
7. S. Nair, H.K. Jeong, A. Chandrasekaran, C. Braunbarth, M. Tsapatis, S.M. Kuznicki, *Chem Mater*, **13**, 4247 (2001).
8. N. V. Zubkova, D. Yu. Pushcharovsky, G. Giester, I. V. Pekov, A. G. Turchkova, N. V. Chukanov, E. Tillmanns, *Crystallogr Rep*, **50**, 367 (2005).
9. N. V. Zubkova, D. Yu. Pushcharovsky, G. Giester, I. V. Pekov, A. G. Turchkova, E. Tillmanns, N. V. Chukanov, *Crystallogr Rep*, **51**, 379 (2006).
10. S. V. Krivovichev, S. N. Britvin, D. V. Spiridonova, V. N. Yakovenchuk, T. Armbruster, in: *Minerals as advanced materials I.* Springer, S. V. Krivovichev (ed.) Heidelberg, 2008, p. 65.

11. D. V. Spiridonova, S. N. Britvin, S. V. Krivovichev, V. N. Yakovenchuk, *Vestnik Sankt-Peterburgskogo Universiteta. Ser Geol Geogr*, (3), 41 (2008) (in Russian).
12. R. Nikolova, B. Shivachev, S. Ferdov, *Microporous and Mesoporous Materials*, **165**, 121 (2013).
13. S. Ferdov, E. Shikova, Z. Ivanova, L. T. Dimowa, R. P. Nikolova, Zhi Lin, B. L. Shivachev, *RSC Advances*, **3** (23), 8843 (2013).
14. L. Tsvetanova, N. Petrova, S. Ferdov, V. Kostov-Kytin, R. Nikolova, *Bulg. Chem. Commun.*, **47**(1), 201 (2015).
15. D. V. Spiridonova, S. V. Krivovichev, S. N. Britvin, V. N. Yakovenchuk, in: *Minerals as Advanced Materials II.*, Springer, S. V. Krivovichev (ed.), Springer Heidelberg New York Dordrecht London, 2011, p. 199.
16. M. Naderi, M. W. Anderson, *Zeolites*, **17**, 437 (1996).
17. J. Rocha, M. W. Anderson, *Eur. J. Inorg. Chem.*, **5**, 801 (2000).
18. S. M. Kuznicki, V. A. Bell, S. Nair, H. W. Hillhouse, R. M. Jacubunas, C. M. Braunbarth, M. H. Toby, M. Tsapatsis, *Nature*, 412, 720 (2001).
19. S. Nair, M. Tsapatsis, B. H. Toby, S. M. Kuznicki, *J. Am. Chem. Soc.*, **123**, 12781, (2001b).
20. S. M. Kuznicki, I. Petrovic, B. T. Desai, *US patent* 6, 068,682 (1990).
21. A. C. Larson, R. B. Von Dreele, General Structure Analysis System (GSAS). Report LAUR 86-748, Los Alamos National Laboratory, 2000.
22. B. H. Toby, *J. Appl. Crystallogr.*, **34**, 210 (2001).
23. S. M. Kuzniki, *US Patent* 6:340–433 (2002).
24. S. M. Kuzniki, *US Patent* 6:517–611 (2003).
25. S. Ferdov, *Langmuir*, **26** (4), 2684 (2010).
26. V. Kostov-Kytin, S. Ferdov, Yu. Kalvachev, B. Mihailova, O. Petrov, *Microporous Mesoporous Mater.*, **105**, 232 (2007).
27. R. P. Nikolova, B. L. Shivachev, S. Ferdov, *Microporous Mesoporous Mater.*, **165**, 121 (2013).
28. T. Roisnel, J. Rodriguez-Carvajal, in: *Materials Science Forum (Proceedings of the Seventh European Powder Diffraction Conference (EPDIC 7))*, R. Delhez and E. J. Mittenmeijer (eds.), 2000, p. 118.
29. K. Momma, F. Izumi, VESTA 3 for three-dimensional visualization of crystal, volumetric and morphology data, *J. Appl. Crystallogr.*, **44**, 1272 (2011).
30. Inorganic Crystal Structure Database (ICSD), Karlsruhe: Gmelin Institute für anorganische Chemie, 2005.